Journal of Materials Chemistry A

PAPER

View Article Online
View Journal | View Issue

Cite this: J. Mater. Chem. A, 2014, 2, 16687

Molecular simulation and experimental study on propylene dehumidification through a PVA–PAA blend membrane

Xiuqin Dong,[ab] Qiao Liu,[ab] Li Cui,[ab] Yingzhe Yu*[ab] and Minhua Zhang*[ab]

Received 18th July 2014
Accepted 6th August 2014

DOI: 10.1039/c4ta03687e

www.rsc.org/MaterialsA

Poly(vinyl alcohol) (PVA) was blended with poly(acrylic acid) (PAA) to improve its separation performance for propylene dehumidification. In this study, molecular simulation was employed to investigate the effect of the PAA content on the properties and separation performance of the membranes. Membrane properties such as density, interaction energy between polymer chains, fractional free volume (FFV), and glass transition temperature (T_g) were analyzed by molecular dynamics (MD) simulation. The adsorption amounts and sites in the membranes were calculated by the Grand Canonical Monte Carlo (GCMC) method. The diffusion process of gas molecules through membranes was also studied both qualitatively and quantitatively by the Einstein relationship. The simulation results showed that the blend membrane exhibits better adsorption performance but lower diffusion coefficient of penetrants than the PVA control membrane. Furthermore, PVA control and PVA–PAA blend membranes were prepared experimentally. The adsorption and separation performance were evaluated. It was found that the changing trend of adsorption was consistent with that of simulation results. The PVA–PAA blend membrane exhibits better separation performance and permeation rate than the PVA control membrane. The permeation rate of gas feed first increased, and then fell down with the increase of the PAA content because of the rate-determining step changed from adsorption to diffusion.

1 Introduction

Gas membrane separation technology has been rapidly adopted industrially over the past few decades because it has many advantages over conventional separation processes (adsorption, absorption and cryogenic distillation) such as high selectivity, low energy consumption, simple process and low investment.[1–3] In recent years, much interest has been centered on the development of high-performance membranes and the relationship between the structure and the separation properties of polymers.[4–7]

Propylene is a significant organic raw material in the petrochemical industry. It should be dehumidified before processed into poly-propylene: the main application of propylene. The propylene–water gas feed was used as a model system in the current study with the main purpose of developing a membrane and exploring the modification method to improve the separation performance.

Gas permeation through polymeric membranes is usually described by the solution-diffusion model. The penetrant molecules firstly adsorb on the high-pressure side of the membrane, then diffuse through the polymeric membranes, and finally desorb from the surface of the low-pressure side of the membrane. Hence, both solubility and diffusivity contribute to the membrane permeability.[8] Therefore, these two processes were performed in this study.

A thin film composite hollow fiber membrane was used in this study due to its high ratios of active surface area-to-volume, low resistance to gas flow, and the ability to withstand high trans-membrane pressure drops.[9,10] A porous polysulfone (PS) hollow fiber was selected as a supporting layer. Poly(vinyl alcohol) (PVA) was chosen as a selective skin layer because of its outstanding hydrophilicity, good mechanical stability, and film forming properties.[11] Although PVA exhibits high separation selectivity, the high crystalline degree results in low penetrability. In order to address this problem, a great deal effort has been devoted to fabricating the PVA control membranes.[12–16] In this study, poly(acrylic acid) (PAA) was blended with PVA to improve membrane dehumidification performance because PAA exhibits a low crystalline degree and –COOH is helpful for the transport of water in the membranes.

Molecular simulation has been applied increasingly widely in polymer science recently.[17–22] The separation mechanism of penetrant molecules in polymer membranes is mainly determined by static structures of membranes at an atomic level and dynamic behavior of small molecules at a picosecond to nanosecond level. But data in this space and time scales are hard to

[a]Key Laboratory for Green Chemical Technology of Ministry of Education Tianjin, Tianjin 300072, China. E-mail: yzhyu@tju.edu.cn; mhzhang@tju.edu.cn; Fax: +86-22-2740-6119; Tel: +86-22-2740-6119

[b]Tianjin University R&D Center of Petrochemical Technology, Tianjin 300072, China

obtain by an experimental study. Molecular simulation is an effective method for researching and predicting the properties of polymer membranes and transport behavior of small penetrant molecules. In recent years, most of the research efforts on the simulation of membrane separation have been focused on the study of its free volume and diffusion coefficient.[23–25]

As far as the authors know, no previous studies have been conducted to explore the structure–performance relationship of PVA–PAA blend membranes for propylene and water separation by combining the simulation method and the experimental method. In the current research, the atomistic models of the PVA control and PVA–PAA blend membranes with various blend ratios were constructed and optimized. The properties of membranes were analyzed, such as density, interaction energy, fractional free volume (FFV), and glass transition temperature (T_g) by MD calculation. Then both GCMC and MD simulation were applied to analyze the effects of adsorption and diffusion processes of gas molecules in membranes with different PAA contents on membrane properties, respectively. Meanwhile, PVA/PS and PVA–PAA/PS hollow fiber composite membranes were prepared and their performance was evaluated experimentally to explore the structure–performance relationship.

2 Details of the simulation

The simulations were carried out using molecular simulation software for materials science, Materials Studio version 4.2, designed by Accelrys, Inc.

In this study, the Polymer Consistent Force Field (PCFF)[26–28] was chosen to calculate interatomic interactions.

Energy minimization was implemented using the smart minimizer method. It starts with steepest-descent to conjugated gradient and then to the Newton–Raphson method as the energy derivative decreases in order to speed up the computation. This protocol ensures that the energy minimization starts with faster convergence and ends up with higher accuracy. For all dynamics runs, the Andersen method[29] was used for temperature control and the Berendsen method[30] for pressure control. A cutoff distance of 9.5 Å, a spline width of 1.0 Å and a buffer width of 0.5 Å were used for all the dynamics runs. The time step was set as 1 fs. The non-bonded energy term was calculated within cut-off distance. Long range Coulomb interactions were calculated by the Ewald sum method.

In our present work, the initial atactic PVA chain was consisted of 200 repetitious units with a 50 : 50 probability for the occurrence of *cis* and *trans* configurations. The packing model contained one energetically minimized PVA chain based on three-dimensional periodic boundary conditions and the packing density was determined from the experimental bulk density of 1.26 g cm^{-3}.[31] Accordingly, the PAA chain consisted of 25 repetitious units. The charge groups of PVA and PAA used in this study were CH, CH_2, OH, and COOH. The configurations of the two chains are shown in Fig. 1.

In order to investigate the effect of PVA and PAA with different blend ratios on the membrane structure and performance, the other four models were also built which contained one PVA chain and 2, 4, 6, and 7 PAA chains, respectively. Ratios

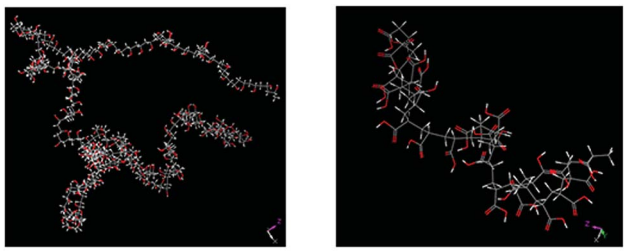

Fig. 1 The configurations of PVA and PAA polymer chains.

by the weight of PVA to PAA in these four cells were 1 : 0.4, 1 : 0.8, 1 : 1.2, and 1 : 1.4 and PAA contents were 28.57 wt%, 44.44 wt%, 54.55 wt%, and 58.33 wt%, respectively. The cells were represented by PVAPAA40, PVAPAA80, PVAPAA120, and PVAPAA140, respectively.

For each of the five membranes, ten independent cells were built and the one with the lowest total energy was chosen for the next calculation. Each of the initial constructed atomistic structure was subjected to the following simulation procedures. Energy minimization was run to eliminate excess overlaps of atoms by the smart minimizer method until the maximum energy deviation became less than 0.001 kcal mol^{-1}. Afterwards, a 50 ps dynamics simulation with the *NVT* ($T = 300$ K) ensemble and 50 ps simulation with the *NPT* ($T = 300$ K, $P = 1.01 \times 10^5$ Pa) ensemble were preliminarily performed to optimize the system energy and configuration. It was generally believed that the system reached equilibrium when parameters such as energy and temperature fluctuated within the range of 5%. The calculation examples are shown in Fig. 2 and 3.

In addition, annealing protocol simulation was used to further optimize the membrane structure. The temperature increased at intervals of 50 K from 300 K to 600 K and at each temperature step 100 ps *NPT* ensemble dynamics run was performed. Then the temperature decreased to 300 K at intervals of 20 K and 250 ps *NPT* run was performed at each step. After subjecting to high temperature to relax the structure, the cells became more stable than before. Finally, 500 ps *NPT* and 500 ps *NVT* dynamics simulations were performed. Atomic coordinates and velocity information were recorded every 1 ps for analyzing the properties of membranes. The five optimized membrane cells are presented in Fig. 4.

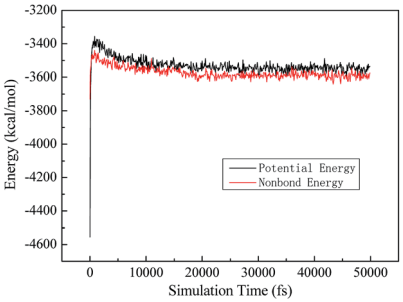

Fig. 2 Potential energy and non-bond energy over simulation time.

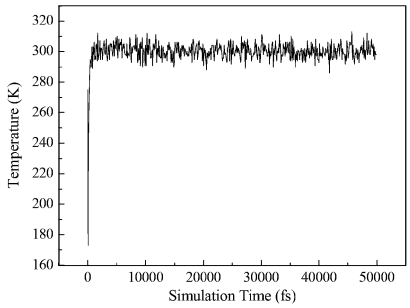

Fig. 3 Temperature over simulation time.

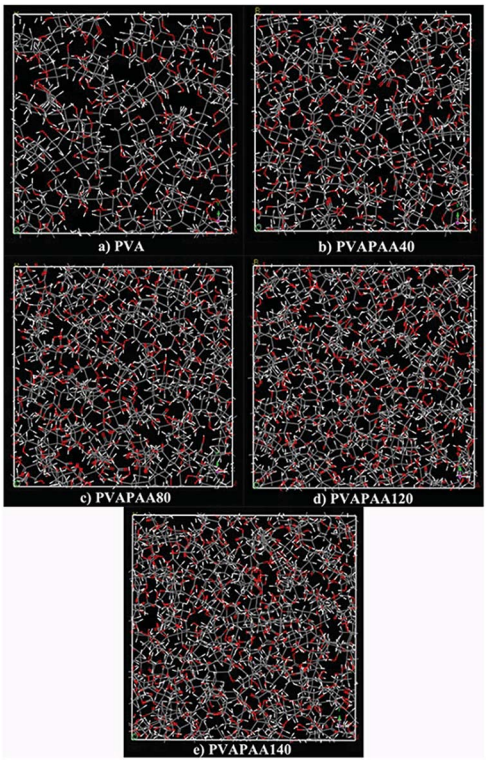

Fig. 4 Optimized models of PVA control and PVA–PAA blend membranes.

In order to verify the accuracy of the selected force field and simulation parameters, the calculated density and solubility parameter values of the PVA control membrane were compared with the experimental results. The reported experimental density of PVA was 1.26 g cm^{-3},[31] while our calculation gave a value of 1.2096 g cm^{-3}. The experimental and calculated solubility parameters were 25.8 and 23.591 $(J\ cm^{-3})^{1/2}$, respectively. The relative deviation of density and solubility parameter were 4.00% and 8.56%, respectively. Such an agreement validated the modeling parameters together with the optimization procedures.

3 Simulation results and discussion

3.1 Calculation of density properties

After optimization, the densities of these membrane models were calculated and the results were 1.2096, 1.2276, 1.2689, 1.2949 and 1.3034 g cm^{-3} in PVA, PVAPAA40, PVAPAA80, PVAPAA120, and PVAPAA140, respectively. The calculated results indicated that the polymer chains of membranes became denser.

3.2 Calculation of interaction energy

The interaction energy ΔE between PVA and PAA polymer chains plays a crucial role in determining the membranes' compatibility and can be calculated as follows:[23,32,33]

$$\Delta E = E_{\text{PVA–PAA}} - (E_{\text{PVA}} + E_{\text{PAA}}) \quad (1)$$

where $E_{\text{PVA–PAA}}$ is the potential energy of the optimized membranes, E_{PVA} and E_{PAA} are the potential energies of individual PVA and PAA polymer chains, respectively. The calculation is based on PCFF. The total energy (E_{total}) consists of non-bond energy ($E_{\text{non-bond}}$) and intra-molecule energy ($E_{\text{intra-molecule}}$). $E_{\text{non-bond}}$ consists of van der Waals energy (E_{vdW}) and Coulomb energy (E_{Coulomb}), in which hydrogen bond energy is included.

$$E_{\text{total}} = E_{\text{non-bond}} + E_{\text{intra-molecule}} \quad (2)$$

$$E_{\text{non-bond}} = E_{\text{vdW}} + E_{\text{coulcomb}} \quad (3)$$

The interaction energy between PVA and PAA was calculated and the results are listed in Table 1.

The values of ΔE are all negative, indicating that the interaction force between PVA and PAA polymer chains is attractive. With the increase of the PAA content, $\Delta E_{\text{non-bond}}$, ΔE_{vdW}, and $\Delta E_{\text{Coulomb}}$ all increase, which indicates that the interaction force between PVA and PAA polymer chains is enhanced. Such results are mainly attributed to two reasons: first, the attractive force shortens the distance between polymer chains; second, a large number of –COOH of PAA can form hydrogen bonds with the –OH of PVA and these hydrogen bonds enhance the interaction.

As shown in Table 1, ΔE_{total} firstly increases and then decreases, and the maximum value appears in membrane PVAPAA120. Both $\Delta E_{\text{non-bond}}$ and $\Delta E_{\text{intra-molecule}}$ contribute to the change of ΔE_{total}. In membrane PVAPAA140, the decrease of $\Delta E_{\text{intra-molecule}}$ becomes the dominant factor which leads to such a phenomenon.

3.3 Calculation of free volume properties

Free volume plays an important role in the transport behavior of penetrant molecules in the membranes. Although some experimental methods, such as positron annihilation lifetime

Table 1 Calculated interaction energy between PVA and PAA in each blend membrane

ΔE (kJ mol^{-1})	PVAPAA40	PVAPAA80	PVAPAA120	PVAPAA140
ΔE_{total}	−3273.07	−4519.12	−6199.65	−5686.85
$\Delta E_{\text{non-bond}}$	−3049.02	−4160.22	−5748.25	−6423.64
ΔE_{vdW}	−1674.88	−2346.65	−3425.89	−3785.93
$\Delta E_{\text{Coulomb}}$	−1374.18	−1813.62	−2342.10	−2637.71

spectroscopy (PALS) and the photochromy method, can be applied to conduct the variances in free volume of membranes experimentally, the techniques are laborious and cannot clearly offer the details about the free volume holes, such as size, size distribution, and morphology. Accurate molecular simulation may solve the problems through systematic free volume characterization.[22]

In this study, the free volume situation of equilibrated PVA control and PVA–PAA blend membranes was analyzed using the "Connolly surface"[34] method as shown in Fig. 5.

The atoms of membranes are represented by hard spheres with van der Waals radius (C, 1.55 Å; H, 1.10 Å; O, 1.35 Å). The fraction of free volume of the PVA control membrane and the equilibrated blend membranes is determined by the radius R_P of a hard spherical probe. The Connolly surface is calculated when the probe molecule rolls over the van der Waals surface, and the free volume is defined as the volume on the side of the Connolly surface without atoms. The FFV is obtained from the ratio of free volume to the total of the model. It should be mentioned that the free volume excludes the volume which is unaccessible by the probe. Since small free volume holes make no big difference to the properties of membranes, accessible free volume holes to penetrant molecules should be more accurate to be in relation to the diffusion properties of the membranes. In this study, the penetrant molecules, water and propylene, were selected as probe molecules which were modeled by spheres with radii of 1.30 Å and 2.35 Å.

From FFV results obtained by each probe molecule in Table 2, it is observed that FFV decreases as the PAA content in membranes increases due to the enhancement of the interaction attractive force which shortens the distance between polymer chains. Accordingly, the density becomes larger and FFV decreases, correspondingly.

Fig. 6 and 7 show the Connolly volume morphology in membranes, and the blue and white colors indicate the accessible volumes. It can be seen that the FFV obtained by a hard spherical probe depends strongly on the size of the probe. It clearly indicates that the FFV decreases as the probe size increases. From Fig. 6 and 7, we can see that the dispersion of free volume holes which are accessible to water are much denser than those holes that are accessible to propylene in blend membranes. It indicates that the dense free volume holes provide a favorable pathway for diffusion of water. Thus, free volume holes that are smaller than water volume did not make considerable contributions to transport properties of the membranes. Therefore, the accessible free volume holes for penetrant molecules should be the major concern.[23] Most of the free volume holes were created by inefficient chain packing or transient gaps caused by chain rearrangement due to their thermal motion. As shown in Fig. 7, stronger interactions between chains of PAA and PVA resulted in a considerable decrease of the size of free volume holes.

Table 2 Free volume properties of PVA control and PVA–PAA blend membranes

Radius (Å)	PVA	PVAPAA40	PVAPAA80	PVAPAA120	PVAPAA140
1.30	8.32	5.85	4.98	4.42	4.37
2.35	0.71	0.27	0.25	0.23	0.14

3.4 Calculation of T_g properties

T_g (glass transition temperature) is a significant property to characterize the mobility or flexibility of polymer chains which can be obtained easily by both molecular simulation and experimental measurements. In this study, T_g was estimated based on the *NPT* ($P = 1.01 \times 10^5$ Pa) ensemble conditions and in a stepwise annealing process.[18] The cell equilibrated at 300 K was heated to 600 K in an interval of 50 K. At each temperature step, 100 ps of *NPT* dynamics run was performed on the cell to reach equilibrium. The cell was then cooled by 20 K each time to 100 K and 250 ps *NPT* run was performed at each step. The first 150 ps dynamics run was used to equilibrate the structure of the

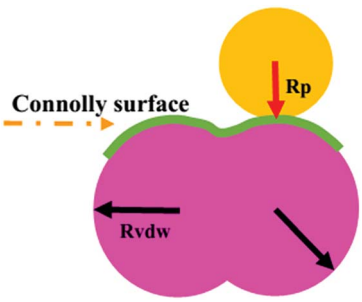

Fig. 5 Schematic diagram for calculating free volume.

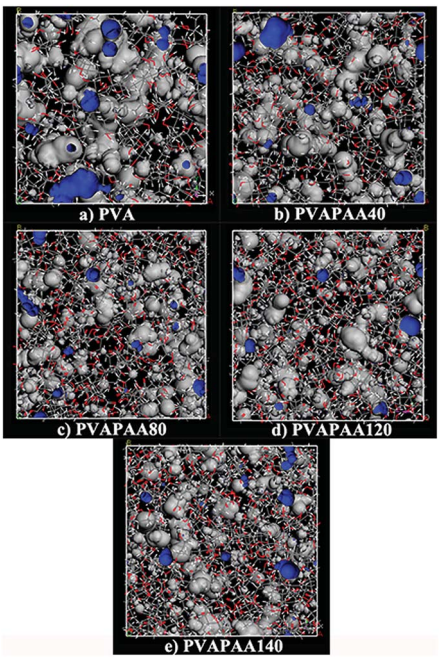

Fig. 6 Simulation of the free volume morphology of PVA and PVA–PAA probed by H_2O.

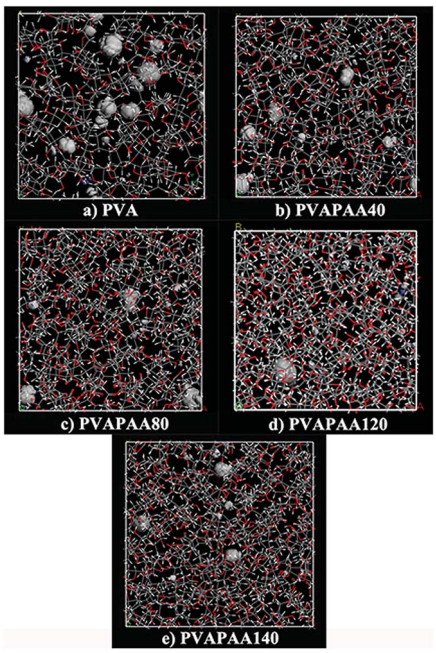

Fig. 7 Simulation of the free volume morphology of PVA and PVA–PAA probed by C_3H_6.

cell and the last 100 ps run was used to determine the specific volume. Specific volumes obtained from *NPT* dynamics for each model were plotted over temperature. The T_gs of these models were determined from the intersection points of the rubbery and glass phase lines.

Fig. 8 illustrates the temperature dependence of the specific volume of different amorphous models. Fig. 9 compares the T_gs

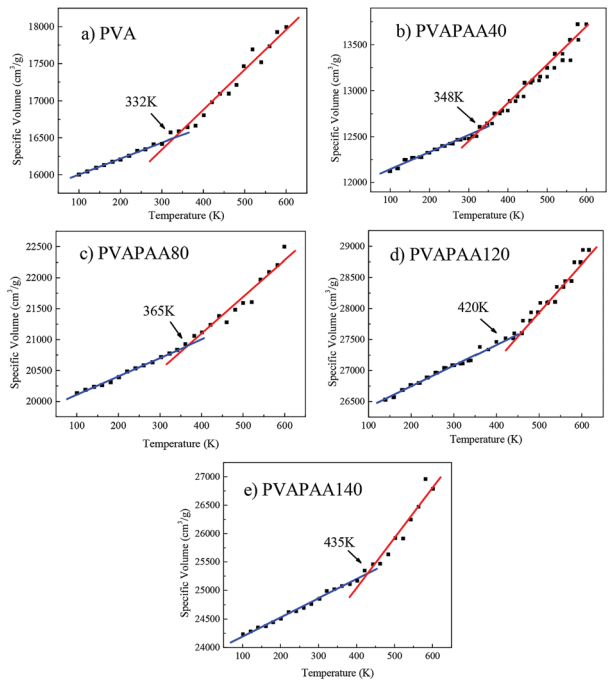

Fig. 8 T_g simulation of PVA control and PVA–PAA blend membranes.

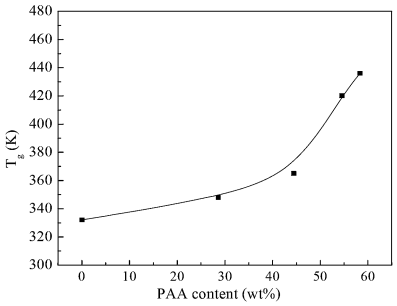

Fig. 9 Effect of the PAA content on T_g.

of PVA control and PVA–PAA blend membranes. The T_g of the PVA control membrane is 332 K, which agrees well with the experimental value of 341.45 K.[35] It can be seen that the T_gs follow the order of PVA < PVAPAA40 < PVAPAA80 < PVAPAA120 < PVAPAA140, and hence polymer chain mobility follows the order of PVA > PVAPAA40 > PVAPAA80 > PVAPAA120 > PVA-PAA140 which is well consistent with the results obtained from analysis of interaction energy and FFV. Higher interaction energy compresses the polymer to higher density, reduces its free volume, and hence limits chain motion to some extent. The lower chain polymer mobility of blend membranes is not conductive to the diffusion process of small penetrants. But higher chain stiffness permits higher selectivity of diffusion. Because there are additional inter-chain interactions, more energy is necessary to overcome attractive forces between chains.[21]

3.5 Calculation of the adsorption process

The study of adsorption in this work was carried out by the sorption module in Materials Studio software. The widely used Grand Canonical Monte Carlo (GCMC) method in adsorption simulation was utilized.[8,18,19]

The simulation was conducted at a fixed pressure of 350 kPa. In the constant pressure simulation, the configurations were sampled from a GC ensemble. The amount and properties of the adsorbed gas molecules in the regions of the polymer matrix were calculated by statistical sampling of molecular configurations at constant μ, V and T. The Metropolis method[36] was employed, in which the trial configurations were generated without bias and the adsorbate structure was treated as rigid. The GCMC calculations were therefore carried out over a single configurational "snapshot" of the polymer system.[37]

The calculation results are shown in Table 3. The adsorption percentage C_S is the mass ratio of adsorbed molecules to the whole model cell. According to the figures, the more PAA content is contained in the membrane, the more adsorption

Table 3 The effect of the PAA content on the adsorption percentage of penetrant molecules in PVA and PVA–PAA membranes

	PVA	PVAPAA40	PVAPAA80	PVAPAA120	PVAPAA140
C_S (wt%)	0.613	0.729	0.794	0.836	0.936

percentage is. The adsorption amounts of water molecules are 3, 5, 7, 9, and 11 in PVA, PVAPAA40, PVAPAA80, PVAPAA120, and PVAPAA140, respectively. The propylene adsorption amount is always 0. According to the amounts, the adsorbed molecules are inserted into the membranes at the calculation adsorption positions which are shown in Fig. 10.

It can be clearly seen from Fig. 10 that blend modification to the PVA membrane is more favorable for water adsorption. It is probably due to the increase of hydrogen bonds between water and –COOH of PAA as the PAA content increases. Since the interaction between carboxyl groups of PAA with water is stronger than hydroxyl groups of PVA, the interaction between the blend membranes and water would increase, and enhance the water uptake naturally.

3.6 Calculation of the diffusion process

The movement of penetrant molecules through the polymer is usually characterized both qualitatively and quantitatively. The thermal vibrations of the polymer chain segments from time to time permit the formation of temporary channels between adjacent voids. These connections can be utilized under suitable conditions for jumps of a penetrant particle from one hole to a neighboring one.[24]

When the condition of an infinitely dilute adsorbate was adopted, only one water molecule was inserted into the optimized PVA membrane model. The intermolecular interactions may be neglected when the number of adsorbate molecules is small.[25] The system was subjected to energy minimization followed by 500 ps *NVT* and 500 ps *NPT* MD simulation. 2000 ps *NVE* ensemble dynamics was then applied by recording all results to analyze the properties. The self-diffusion coefficient was calculated as follows:

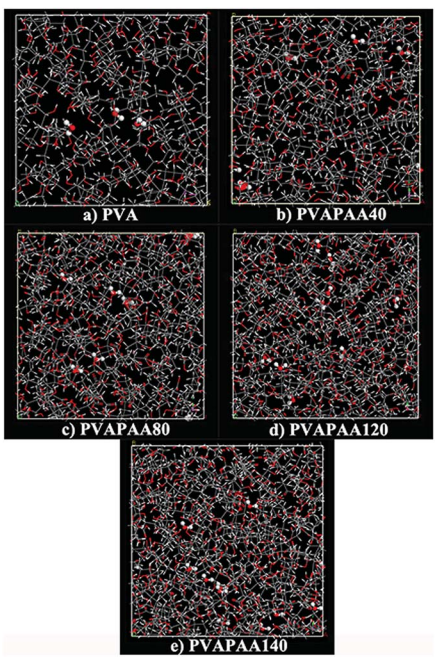

Fig. 10 Adsorption models of membrane cells with penetrant molecules.

$$D_S = \lim_{t\to\infty} \frac{1}{6t} \left\langle \left| \vec{r}(t) - \vec{r}(0) \right|^2 \right\rangle \quad (4)$$

where D_S is the self-diffusion coefficient of the molecule, $\vec{r}(0)$ is the initial position vector, $\vec{r}(t)$ is its position vector at time t, and $\langle|\vec{r}(t) - \vec{r}(0)|^2\rangle$ is the MSD.

The time courses of the MSD in the first 200 ps were recorded to analyze the mechanism of small molecule diffusion in the membrane qualitatively. As illustrated in Fig. 11, three types of movement of water molecules in the membrane can be clearly seen:[18] first, the initial raise of the plot represents diffusion through channels; second, the intermediate section represents jumping back from one void to another; and the third section represents the penetrant trapped in a void. It should be mentioned that the back "jump" exists, but only the forth "jump" contributes to and facilitates the diffusion process.

In order to further study the diffusion behavior of the penetrant molecules in the membranes with different ratios of PAA to PVA, penetrant molecules (only water molecules were adsorbed) were inserted into the models of membranes according to the adsorption amount at the calculation positions. The systems were initially allowed to equilibrate by energy minimization followed by 500 ps *NVT* and 500 ps *NPT* MD simulation. The final systems were subjected to another 2000 ps *NVE* dynamics by recording all results. The time step was set as 1 fs. Atomic coordinates and velocity information were recorded every 1000 steps (1 ps) during dynamics for later analysis. The mean-square displacement (MSD) obtained from the simulations was used to analyze the diffusion coefficients by the Einstein equation:

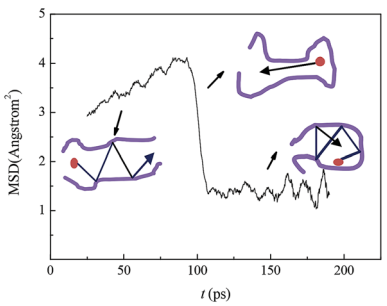

Fig. 11 MSD trajectory and motions of small molecules in membranes.

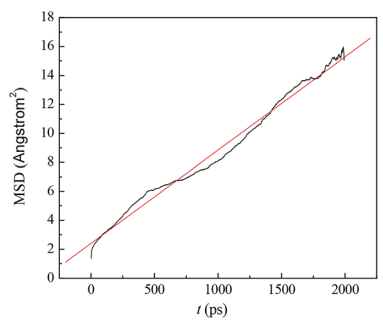

Fig. 12 The diffusion coefficient of water molecules in the membrane.

Table 4 The diffusion coefficients of water in PVA control and PVA–PAA blend membranes

	PVA	PVAPAA40	PVAPAA80	PVAPAA120	PVAPAA140
D_{H_2O} ($\times 10^{-11}$ m^2 s^{-1})	16.33	10.50	6.83	6.17	4.99

$$D_i = \frac{1}{6}\lim_{t\to\infty}\frac{d}{dt}\sum_{i=1}^{N}\left\langle\left|\vec{r}_i(t)-\vec{r}_i(0)\right|^2\right\rangle \quad (5)$$

where D_i is the diffusion coefficient of i penetrant, $\vec{r}_i(0)$ is its initial position vector, $\vec{r}_i(t)$ is its position vector at time t, and $\langle|\vec{r}_i(t) - \vec{r}_i(0)|^2\rangle$ is the MSD of i penetrant. The diffusion coefficient was the average value of all penetrant molecules.

Fig. 12 shows the diffusion coefficient of water molecules in the membrane. It can be seen that 2000 ps is long enough for this system to calculate the diffusion coefficient.

Table 4 shows the changing trend of diffusion coefficient as a function of PAA content in membranes. The diffusion coefficient of the PVA control membrane is larger than that of the PVA–PAA blend membrane and follows the order of PVA > PVAPAA40 > PVAPAA80 > PVAPAA120 > PVAPAA140. The diffusion of water in the membranes is strongly dependent on the free volume, the chain mobility and polymer–water interactions. The size, distribution and connectivity of free volume holes would all influence the penetrant diffusion. The higher of the FFV is, the more accessible holes there are for the penetrant to diffuse into the membranes. When there are plenty of free volume holes in the membranes, the penetrant molecules need a shorter path jumping from one hole to the neighbouring ones. The diffusion coefficient is correlated with the FFV. As shown in Fig. 13, diffusion coefficients have an exponential relation to 1/FFV, which agrees well with the commonly employed free volume theory.[32,38]

$$\log D_i = A - \frac{B}{\mathrm{FFV}_i} \quad (6)$$

where A and B are constants for certain penetrants.

As analyzed above, the FFV and chain mobility become poorer as the PAA content in membranes increases, which does not facilitate the transfer of small molecules. Lower FFV provides smaller free volume holes which water molecules could "jump" to. And higher stiff of polymer chains indicates the channels that small molecules diffuse into are not flexible to form and close.

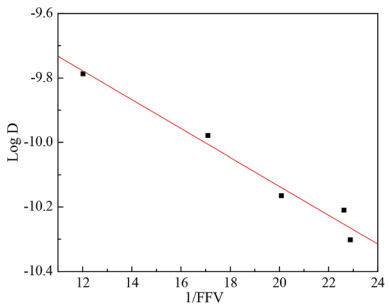

Fig. 13 Correlation between log D and 1/FFV.

The simulation results show that blend modification is helpful to improve separation factors of membranes for the propylene and water system. And blend modification enhances the affinity between water and membranes, which is favorable for the permeation rate. But the permeation rate is influenced by adsorption and diffusion processes, and there might be an appropriate value of a blend ratio of PVA to PAA.

4 Experimental

4.1 Preparation of hollow fiber composite membranes

In the following experiment, hollow fiber composite membranes were utilized. A polysulfone (PS) hollow fiber with a molecular weight cut off of 30 000 (from Tianjin Motian Membrane Engineering and Technology Co., Ltd) and PVA (from Tianjin Yuanli Chemical Company in China, polymerization degree of 1750 ± 50, 99+% hydrolyzed) were dissolved in distilled water at 363 K and stirred for about 1 h to obtain 5 wt% solutions, and then cooled to room temperature. A certain amount of PAA (molecular weight 5000 Dalton, from Shandong Taihe Water Treatment Co., Ltd.) was added into PVA solutions according to the blend ratios used in the molecular simulation. Then PS base membranes with the glycerol coating already removed were soaked into the solutions and hung to dry for about 2 h at room temperature. The hollow fiber composite membranes were spread twice and hung upside down to ensure that the thickness of the active layer was uniform. Six hollow fiber composite membranes were installed into the membrane module. The effective surface area in contact with gas feed in this membrane module was 16.24 cm^2.

4.2 Adsorption experiment

A certain mass (m_0) of hollow fiber membranes was weighed out and subjected to vacuum drying. Then gas feed with a humidity of 0.6 wt% blew through the membranes in a sealed container for 24 h. The membranes were taken out and the mass changed to m_t. The adsorption percentage C_E was calculated as follows:

$$C_E = \frac{m_t - m_0}{m_0}\times 100\% \quad (7)$$

As shown in Fig. 14, the adsorption amount of small molecules in membranes becomes larger as the PAA content increases. We attributed the results to the strongly hydrophilic characteristic of blend membranes with more PAA incorporated into PVA forming hydrogen bonds between –COOH of PAA and H_2O thus promoting the adsorption of water.

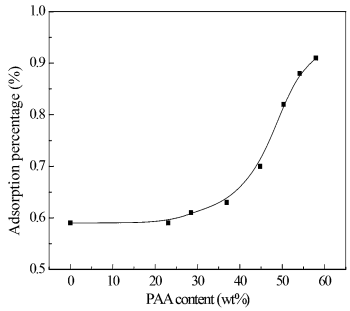

Fig. 14 Effect of the PAA content on adsorption amounts of penetrant molecules.

4.3 Gas separation performance tests

The humidity of water–propylene gas feed was 0.6 wt%. A feed pressure of 350 kPa was applied to the shell side of the fibers, and the permeation side was swept by highly pure nitrogen (99.999+% pure) and the pressure was maintained at about 180 kPa. The operation temperature was 298 K. The flowing rates of gas feed and nitrogen were 200 and 100 cm^3 (STP) per minute, respectively. The compositions of the feed and permeate were measured by Agilent 6820 (USA) gas chromatography with a TCD detector. The separation performance of the membranes was evaluated by two parameters: permeation rate $(P/l)_i$ and separation factor $\alpha_{i/j}$.

$$\left(\frac{P}{l}\right)_i = \frac{Q_i}{\Delta P_i A} \tag{8}$$

$$\alpha_{H_2O/C_3H_6} = \frac{(P/l)_{H_2O}}{(P/l)_{C_3H_6}} \tag{9}$$

where Q_i is the volume flow rate of i gas at standard temperature and pressure (STP), ΔP_i is the trans-membrane pressure difference, and A is the membrane active surface area. The permeance is expressed in gas permeation units, GPU (1 GPU = 10^{-6} cm^3 (STP) cm^{-2} s^{-1} $cmHg^{-1}$).

The effect of the PAA content on the membrane permeation rate is investigated and the results are shown in Fig. 15. As expected, the permeation rates of the blend membranes are larger than those of the PVA control membrane (153.41 GPU). Permeation rates of PVAPAA increase initially with the PAA content (from 0 to 54.55 wt%) in the blend membranes and reach the maximum value of 322.6 GPU when the PAA content is 54.55 wt%, and then decrease with further introduction of PAA into the blend membranes. From molecular simulation perspective, the adsorption amount increases, but the diffusion coefficient of water molecules becomes smaller as the PAA content increases in the membranes. According to the well-known adsorption–diffusion mass transfer mechanism, the permeation rate is influenced by both adsorption and diffusion processes of penetrants. The adsorption process plays a dominant role when the PAA content is lower than 54.55%, while the diffusion process seems to become the dominant factor when the PAA content is higher than 54.55%. This explains the phenomenon that the permeation rate decreases and PVA-PAA120 exhibits the largest permeation rate.

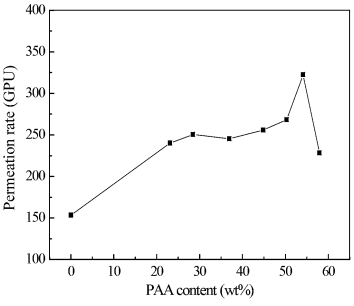

Fig. 15 Effect of the PAA content on the gas permeation rate through membranes.

The separation factor is also an important parameter to evaluate the membrane performance. In this study, the separation factor of the PVA control membrane was 25 202. For PVA–PAA blend membranes, propylene could not be detected in the permeation side so the separation factor was extremely large (as for blend membranes, the permeation rate of gas feed is the permeation rate of water) Through microcosmic perspective, higher packing density, lower free volume holes, and higher stiff of polymer chains naturally caused higher selectivity. In addition, hydrogen bonds between water molecules and the polymer chains could be formed in this material, which also increased the interaction and, hence, the selectivity.[20]

5 Conclusions

Both molecular simulation and experimental study methods were employed to investigate the effects of blend modification and different blend ratios of PAA to PVA on the membrane structural morphology and separation performance of the water–propylene system. The simulation results showed that with the increasing content of PAA, the membrane density increases, the attractive force between polymer chains becomes stronger, the fractional free volume of membranes decreases and glass transition temperature becomes higher. Through the calculation of adsorption and diffusion of propylene and water in membranes, it was observed that more PAA was contained in the membrane, and more penetrants were adsorbed. The diffusion coefficients were smaller in the membrane with a higher PAA content which was due to the lower FFV and chain mobility. It was also observed that diffusion coefficients had an exponential relation to 1/FFV.

Meanwhile, PVA/PS and PVA–PAA/PS hollow fiber composite membranes were prepared and the performances were evaluated experimentally. The results showed that the adsorption amount of gas feed in membranes became larger, and the permeation rate of gas feed firstly increased, and then fell down with the increase of the PAA content in the membranes. It was noted that the maximum permeation rate appeared at the membrane with the PVA–PAA ratio of 1 : 1.2. The permeation rate increased from 153.41 GPU of the PVA control membrane to 322.60 GPU. From microcosmic perspective, this is because the adsorption process plays a dominant role when the PAA

content is low while the diffusion process plays a dominant role when the PAA content is high. The separation factor increases from 25 202 to infinity.

The results showed that PVA–PAA blend membranes exhibited better performance than the PVA control membrane. The calculation results agree well with experimental results. It indicates that the molecular simulation method had a high value in analyzing microscopic properties of membranes, exploring the affinity between the gas and the membrane, and predicting the permeation rate and separation factor.

Nomenclature

A	Surface area of membranes, m^2
$\alpha_{i/j}$	Separation factor
C_E	Adsorption percentage of the experiment, %
C_S	Adsorption percentage of molecular simulation, %
D_S	Self-diffusion coefficient, $m^2\ s^{-1}$
D_i	Diffusion coefficient of i penetrant, $m^2\ s^{-1}$
ΔE	Interaction energy, kJ mol^{-1}
E_{total}	Total energy, kJ mol^{-1}
$E_{non\text{-}bond}$	Non-bond energy, kJ mol^{-1}
E_{vdW}	van der Waals energy, kJ mol^{-1}
$E_{Coulomb}$	Coulomb energy, kJ mol^{-1}
$E_{PVA\text{–}PAA}$	Potential energy of the PVA–PAA blend membrane, kJ mol^{-1}
E_{PVA}	Potential energy of the optimized PVA polymer chain, kJ mol^{-1}
E_{PAA}	Potential energy of the optimized PAA polymer chain, kJ mol^{-1}
FFV	Fraction of the free volume, %
MSD	Mean-square displacement, $Å^2$
P	Pressure, Pa
$(P/l)_i$	Permeation rate of i penetrant, GPU
R_p	Radius of the probe molecular, Å
$r_i(t)$	Positions of atoms i at time t
$r_i(0)$	Positions of atoms i at time 0
T	Temperature, K
T_g	Glass transition temperature
t	Time, ps

Notes and references

1 J. T. Chen, Y. J. Fu, K. L. Tung, Sh. H. Huang, W. S. Hung, Sh. J. Lue, C. C. Hu, K. R. Lee and J. Y. Lai, Surface modification of poly(dimethylsiloxane) by atmospheric pressure high temperature plasma torch to prepare high-performance gas separation membranes, *J. Membr. Sci.*, 2013, **440**, 1–8.

2 N. Y. Du, H. B. Park, M. M. Dal-Cin and M. D. Guiver, Advances in high permeability polymeric membrane materials for CO_2 separations, *Energy Environ. Sci.*, 2012, **5**, 7306–7322.

3 B. Zhang, T. H. Wang, Y. H. Wu, Q. L. Liu, S. L. Liu, Sh. H. Zhang and J. Sh. Qiu, Preparation and gas permeation of composite carbon membranes from poly(phthalazinone ether sulfone ketone), *Sep. Purif. Technol.*, 2008, **60**, 259–263.

4 Sh. H. Li, H. J. Jo, S. H. Han, C. H. Park, S. J. Kim, P. M. Budd and Y. M. Lee, Mechanically robust thermally rearranged (TR) polymer membranes with spirobisindane for gas separation, *J. Membr. Sci.*, 2013, **434**, 137–147.

5 Q. G. Zhang, Q. L. Liu, Sh. P. Huang, W. W. Hu and A. M. Zhu, Microstructure-related performances of poly(vinyl alcohol)–silica hybrid membranes: a molecular dynamics simulation study, *J. Mater. Chem.*, 2012, **22**, 10860–10866.

6 W. S. Chi, S. U. Hong, B. Jung, S. W. Kang, Y. S. Kang and J. H. Kim, Synthesis, structure and gas permeation of polymerized ionic liquid graft copolymer membranes, *J. Membr. Sci.*, 2013, **443**, 54–61.

7 C. Sanchez, B. Julian, P. Belleville and M. Popall, *J. Mater. Chem.*, 2005, **15**, 3559–3592.

8 K. L. Tung, K. T. Lu, R. C. Ruaan and J. Y. Lai, MD and MC simulation analyses on the effect of solvent types on accessible free volume and gas sorption in PMMA membranes, *Desalination*, 2006, **192**, 391–400.

9 E. K. Chatzidaki, E. P. Favvas, S. K. Papageorgiou, N. K. Kanellopoulos and N. V. Theophilou, New polyimide–polyaniline hollow fibers: Synthesis, characterization and behavior in gas separation, *Eur. Polym. J.*, 2007, **43**, 5010–5016.

10 N. Widjojo, Sh. H. D. Zhang, T. Sh. Ch and Y. Liu, Enhanced gas separation performance of dual-layer hollow fiber membranes via substructure resistance reduction using mixed matrix materials, *J. Membr. Sci.*, 2007, **306**, 147–158.

11 A. K. Sahu, G. Selvarani, S. D. Bhat, S. Pitchumani, P. Stridhar, A. K. Shukla, N. Narayanan, A. Banerjee and N. Chandrakumar, Effect of varying poly(styrene sulfonic acid) content in poly(vinyl alcohol)-poly(styrene sulfonic acid) blend membrane and its ramification in hydrogen–oxygen polymer electrolyte fuel cells, *J. Membr. Sci.*, 2008, **319**, 298–305.

12 Q. L. Cheng, F. Sh. Pan, B. Chen and Zh. Y. Jiang, Preparation and dehumidification performance of composite membrane with PVA/gelatin–silica hybrid skin layer, *J. Membr. Sci.*, 2010, **363**, 316–325.

13 M. Jahanshahi, A. Rahimpour and N. Mortazavian, Preparation, morphology and performance evaluation of polyvinylalcohol (PVA)/polyethersulfone (PES) composite nanofiltration membranes for pulp and paper wastewater treatment, Ira, *Polym. J.*, 2012, **21**, 375–383.

14 Q. G. Zhang, Q. L. Liu, Z. Y. Jiang and Y. Chen, Anti-trade-off in dehydration of ethanol by novel PVA/APTEOS hybrid membranes, *J. Membr. Sci.*, 2007, **287**, 237–245.

15 H. K. Yuan, J. Ren, X. H. Ma and Zh. L. Xu, Dehydration of ethyl acetate aqueous solution by pervaporation using PVA/PAN hollow fiber composite membrane, *Desalination*, 2011, **280**, 252–258.

16 Q. G. Zhang, Q. L. Liu, Y. Chen and J. H. Chen, Dehydration of Isopropanol by Novel Poly(vinyl alcohol)–SiliconeHybrid Membranes, *Ind. Eng. Chem. Res.*, 2007, **46**, 913–920.

17 F. Sh. Pan, J. Ma, L. Cui and Zh. Y. Jiang, Water vapor/propylene sorption and diffusion behavior in PVA–P(AA-AMPS) blend membranes by GCMC and MD simulation, *J. Membr. Sci.*, 2009, **64**, 5192–5197.

18 K. L. Tung and K. T. Lu, Effect of tacticity of PMMA on gas transport through membranes: MD and MC simulation studies, *J. Membr. Sci.*, 2006, **272**, 37–49.

19 M. Heuchel, D. Fritsch, P. M. Budd, N. B. McKeown and D. Hofman, Atomistic packing model and free volume distribution of a polymer with intrinsic microporosity (PIM-1), *J. Membr. Sci.*, 2008, **318**, 84–99.

20 C. Nagel, E. Schmidtke, K. Günther-Schade, D. Hofman, D. Fritch, T. Strunskus and F. Faupel, Free Volume Distributions in Glassy Polymer Membranes: Comparison between Molecular Modeling and Experiments, *Macromolecules*, 2000, **33**, 2242–2248.

21 Y. Tamai, H. Tanaka and K. Nakanishi, Molecular simulation of permeation of small penetrants through membranes, diffusion coefficients, *Macromolecules*, 1994, **27**, 4498–4508.

22 S. S. Jawalkar, S. G. Adoor, M. Sairam, M. N. Nadagouda and T. M. Aminabhavi, Molecular Modeling on the Binary Blend Compatibility of Poly(vinyl alcohol) and Poly(methyl methacrylate): An Atomistic Simulation and Thermodynamic Approach, *J. Phys. Chem. B*, 2005, **109**, 15611–15620.

23 K. Sh. Chang, Y. H. Huang, K. R. Lee and K. L. Tung, Free volume and polymeric structure analyses of aromatic polyamide membranes: A molecular simulation and experimental study, *J. Membr. Sci.*, 2010, **354**, 93–100.

24 F. Sh. Pan, F. B. Peng and Zh. Y. Jiang, Diffusion behavior of benzene/cyclohexane molecules in poly(vinyl alcohol)–graphite hybrid membranes by molecular dynamics simulation, *Chem. Eng. Sci.*, 2007, **62**, 703–710.

25 J. Zh. Yang, Q. L. Liu and H. T. Wang, Analyzing adsorption and diffusion behaviors of ethanol/water through silicalite membranes by molecular simulation, *J. Membr. Sci.*, 2007, **291**, 1–9.

26 H. Sun, S. J. Mumby, J. R. Maple and A. T. Hagler, An ab initio CFF93 all-atom force field for polycarbonates, *J. Am. Chem. Soc.*, 1994, **116**, 2978–2987.

27 M. J. Hwang, T. P. Stockfisch and A. T. Hagler, Derivation of class II force fields. 2. Derivation and characterization of a class II force field, CFF93, for the alkyl functional group and alkane molecules, *J. Am. Chem. Soc.*, 1994, **116**, 2515–2525.

28 H. Sun, *Ab initio* calculations and force field development for computer simulation of polysilanes, *Macromolecules*, 1995, **28**, 701–712.

29 T. A. Andrea, W. C. Swope and H. C. Andersen, The role of long ranged forces in determining the structure and properties of liquid water, *J. Chem. Phys.*, 1983, **79**, 4576–4584.

30 H. J. C. Berendsen, J. P. M. Postma, W. F. van Gunsteren, A. DiNola and J. R. Haak, Molecular dynamics with coupling to an external bath, *J. Chem. Phys.*, 1984, **81**, 3684–3690.

31 R. L. Davidson, *Handbook of Water-soluble Gums and Resins*, McGraw-Hill, New York, 1980.

32 F. Sh. Pan, F. B. Peng, L. Y. Lu, J. T. Wang and Zh. Y. Jiang, Molecular simulation on penetrants diffusion at the interface region of organic–inorganic hybrid membranes, *Chem. Eng. Sci.*, 2008, **63**, 1072–1080.

33 B. Li, F. Sh. Pan, Zh. P. Fang, L. Liu and Zh. Y. Jiang, Molecular Dynamics Simulation of Diffusion Behavior of Benzene/Water in PDMS-Calix[4]arene Hybrid Pervaporation Membranes, *Ind. Eng. Chem. Res.*, 2008, **47**, 4440–4447.

34 M. L. Connolly, Computation of molecular volume, *J. Am. Chem. Soc.*, 1985, **107**, 1118–1124.

35 H. P. Jia, *Blended sodium alginate composite membranes for dehumidification of propylene*, 2009.

36 N. Metropolis, A. W. Rosenbluth, M. N. Rosenbluth, A. H. Teller and E. Teller, *J. Chem. Phys.*, 1953, **21**, 1087–1092.

37 S. W. Rutherford, D. T. Limmer, M. G. Smith and K. G. Honnjell, Gas transport in ethylene-propylene-diene (EPDM) elastomer: Molecular simulation and experimental study, *Polymer*, 2007, **48**, 6719–6727.

38 X. Y. Wang, P. J. Veld, Y. Lu, B. D. Freeman and I. C. Sanchez, A molecular simulation study of cavity size distributions and diffusion in para and meta isomers, *Polymer*, 2005, **46**, 9155–9161.

